JOURNAL OF GEOPHYSICAL RESEARCH, VOL. 113, B04401, doi:10.1029/2007JB005194, 2008

Modeling GPS phase multipath with SNR: Case study from the Salar de Uyuni, Boliva

Andria Bilich,[1] Kristine M. Larson,[2] and Penina Axelrad[2]

Received 30 May 2007; revised 30 October 2007; accepted 18 December 2007; published 1 April 2008.

[1] Multipath, wherein a signal arrives at the receiving antenna by more than one path, is a significant and largely unmodeled source of GPS positioning error. We present a technique for mitigating specular multipath in GPS carrier phase measurements using the signal-to-noise ratio (SNR), in which the frequency and amplitude content of non-stationary oscillations in SNR are modeled to extract multipath parameters (direct and reflected signal amplitudes, and the phase difference between direct and indirect signals). The frequency content of SNR data is estimated using wavelet analysis, then used to initialize an adaptive least squares process to solve for time-varying multipath parameters. Multipath corrections derived from these parameters are applied to the phase observables. We demonstrate this technique using campaign GPS data collected over a large salt flat (Salar de Uyuni), specifically a tripod-mounted station which experienced long-period (300–2000 s) multipath oscillations in SNR from ground reflections. By contrasting position solutions before and after applying multipath corrections, we demonstrate a reduction in carrier phase postfit residual RMS of up to 20% for static positioning, and 1–7 dB reduction in spectral power at multipath periods for kinematic positions.

Citation: Bilich, A., K. M. Larson, and P. Axelrad (2008), Modeling GPS phase multipath with SNR: Case study from the Salar de Uyuni, Boliva, *J. Geophys. Res.*, *113*, B04401, doi:10.1029/2007JB005194.

1. Introduction

[2] A precise model for the carrier phase observable is crucial to high-precision Global Positioning System (GPS) applications such as geodesy. Although many GPS model improvements have been made in the last decade [e.g., *Springer et al.*, 1998; *Mader*, 1999; *Altamimi et al.*, 2002; *Kedar et al.*, 2003], to date there is no accepted model to account for multipath effects, specifically the effects of specular multipath (reflections from a smooth surface resulting in slowly varying systematic errors) on the GPS carrier phase. Specular multipath leads to positioning errors whether position is computed at every epoch [*Larson et al.*, 2007; *Choi et al.*, 2004; *Bock et al.*, 2000] or a single position is determined from 24 h of data [*Elosegui et al.*, 1995]. In high multipath environments these range errors can be substantial, on the order of meters for pseudorange and several centimeters for phase [*Braasch*, 1996].

[3] Our method for modeling and correcting carrier phase multipath relies on signal-to-noise ratio (SNR) data. Earlier studies incorporated SNR measurements in correcting carrier phase multipath in aerospace environments [*Comp and Axelrad*, 1997; *Reichert*, 1999; *Reichert and Axelrad*, 1999] with a master and several slave antennas in a closely spaced array, i.e., differential multipath. *Comp and Axelrad* [1997] demonstrated how differential carrier phase multipath could be reduced up to 47% by modeling the frequency and amplitude content of differential SNR. *Ray* [2000] and *Ray and Cannon* [2001] developed a method for jointly filtering single-differenced measurements of code, carrier phase, and SNR to determine multipath parameters. Subsequent multipath corrections resulted in an average of 22% and 15% reduction in code and carrier residuals, respectively. Accuracy was improved by 21% and 24% for differential code and carrier positioning, respectively.

[4] This study adapts the differential-multipath methodology to undifferenced carrier phase data so that the method can be applied to the stand-alone GPS stations commonly used in geodetic networks. For this type of application, an effective phase multipath mitigation technique would take into account a number of features unique to geodetic and CGPS sites, networks, and archives: solitary GPS antennas located in both rural and urban environments; the variety of existing GPS receiver models; antenna orientations with little below-horizon ($<0^\circ$) observability of GPS satellites; and large existing archives of GPS data with variable sample intervals. Thus this study establishes a technique to correct single-station phase multipath using undifferenced observables. This technique is not receiver-specific nor designed specifically for real-time operation. It could potentially be applied to various models and types of GPS receivers using observables already available in archived data.

[5] The paper first outlines the relationships between SNR and phase multipath, and demonstrates how multipath errors in carrier phase observables are a function of the

[1]National Geodetic Survey, Boulder, Colorado, USA.
[2]Department of Aerospace Engineering Sciences, University of Colorado, Boulder, Colorado, USA.

0148-0227/08/2007JB005194$09.00

Table 1. Summary of Symbols Used for Multipath Terms

Symbol	Term	Units
Amplitudes		
A_m	multipath signal amplitude	volts
A_d	direct signal amplitude	volts
α	amplitude ratio of multipath to direct; $\alpha = A_m/A_d$	unitless
Angles		
ψ	multipath relative phase; phase difference between indirect and direct signals	radians
θ	satellite elevation angle, relative to local horizontal	radians
β	angle of reflection	radians
γ	angle of reflector tilt, relative to local horizontal	radians
Errors		
δ	path delay; additional path length traveled by indirect signal relative to the direct	meters
ρ_{MP}	pseudorange error due to multipath	meters
$\delta\phi$	carrier phase error due to multipath	cycles

frequency and amplitude content of SNR data. SNR data are used to generate profiles of carrier phase multipath for individual satellites, and the profiles are subsequently used to remove carrier phase multipath errors. Least squares position solutions with and without the correction profiles are then computed and evaluated. The advantages and limitations of this technique in the context of a simplified multipath environment are also discussed.

2. SNR and Carrier Phase Multipath Theory

[6] This section uses terminology specific to GPS multipath, which is summarized here and in Table 1. In a multipath-free environment, the receiver intercepts signals traveling a direct path between the GPS satellites and a receiver, so that the single-channel signal power is equivalent to the direct signal amplitude, denoted A_d for an individual satellite. Upon reflection from a surface, an indirect signal is attenuated so that its amplitude A_m is less than the direct, i.e., $A_m \leq A_d$. In some cases it is useful to describe the multipath and direct amplitudes as a ratio, $\alpha = A_m/A_d$. Because reflected signals arrive by an indirect path, the reflected signal has a longer path length than the direct. This additional path length, referred to as the path delay (δ), creates a range error, which subsequently leads to a positioning error. The phase multipath error is expressed as $\delta\phi$, in units of cycles. The reflected signal's carrier wave, upon reception by the GPS antenna, will likely have a different phase than the direct signal; the difference in the phases of the two signals is described as the multipath relative phase, ψ.

[7] Although derivations of the exact multipath-SNR relationships have been given by many others [*Axelrad et al.*, 2005; *Ray*, 2000; *Comp*, 1996; *Georgiadou and Kleusberg*, 1988], the salient equations are summarized here to demonstrate that, in theory, the frequency and amplitude content of SNR data are directly related to carrier phase multipath errors. We direct the reader to *Bilich and Larson* [2007] for precise derivations and additional background material. Under the simplified model of GPS signal tracking in the presence of direct and reflected signals, multipath-SNR equations can be derived which express the phase error $\delta\phi$ and the signal-to-noise ratio S in terms of the multipath parameters (Table 1):

$$\tan(\delta\phi) = \frac{A_m \sin\psi}{A_d + A_m \cos\psi} \tag{1}$$

$$S^2 = A_d^2 + A_m^2 + 2A_dA_m \cos\psi \tag{2}$$

Because the time-dependent behavior of both these quantities is dominated by the sine or cosine of ψ, it is important to understand the time-dependency of the multipath relative phase. As discussed by *Comp* [1996] and *Bilich and Larson* [2007], ψ is a function of the receiver-satellite geometry (Figure 1): the perpendicular antenna-reflector distance h and several angles measured relative to local horizontal, i.e., the angle of reflection at the surface β, the satellite elevation angle θ, and reflector tilt γ:

$$\psi = \frac{2\pi}{\lambda} 2h \sin\beta \tag{3}$$

$$\psi = \frac{2\pi}{\lambda} 2h \sin(|\theta - \gamma|) \tag{4}$$

where λ is the GPS wavelength. Note that the absolute value in equation (4) is a general formulation of β which

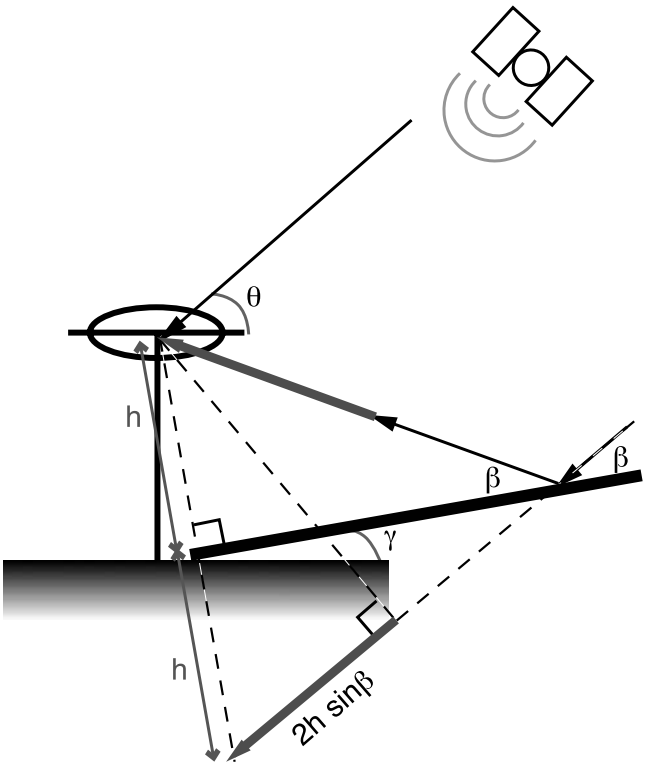

Figure 1. Geometry of a forward-scatter specular multipath reflection from a planar surface tilted at angle γ and located at a distance h from the antenna phase center. The angle of incidence β at the surface is equivalent to the angle of reflection, and θ is the satellite elevation angle. Bold arrows show the additional path length ($\delta = 2h\sin\beta$) traveled by the multipath signal relative to the direct. All objects are considered coplanar (no third dimension), and all angles are defined relative to local horizotal.

holds true for both forward (Figure 1) and backscatter geometries [*Bilich*, 2006]. By assuming reflecting objects persist so that γ and h are constant, the only time-dependent factor remaining in equation (4) is the satellite motion (satellite elevation angle). Taking the time-derivative of ψ:

$$\frac{d\psi}{dt} = \frac{2\pi}{\lambda} 2h \cos(\theta - \gamma) \left| \frac{d\theta}{dt} \right| \quad (5)$$

As will be shown below, the sign of $d\psi/dt$ must be unambiguous for proper computation of multipath phase corrections. If we assume that γ is both time-invariant and so small as to be negligible compared to θ, $\beta \cong \theta$ and $d\beta/dt \cong d\theta/dt$. Thus the time-derivative of equation (3) becomes:

$$\omega \equiv \frac{d\psi}{dt} = \frac{2\pi}{\lambda} 2h \cos\theta \frac{d\theta}{dt} \quad (6)$$

By assuming multipath reflections originate from flat ground or low-angle surfaces, resulting in a purely forward-scatter geometry, the sign of $\omega \equiv d\psi/dt$ is determined simply by recognizing if the satellite is ascending or descending as a function of time. Therefore this study seeks to model only ground multipath reflections with small γ because the sign of $d\psi/dt$ for flat ground reflections is well-understood.

3. Multipath Estimation Methodology

[8] In order to correct for multipath on the GPS carrier phase, amplitudes A_m and A_d and multipath relative phase ψ must be estimated as a function of time. The previous section provided the theoretical underpinnings of the relationship between SNR and phase multipath; this section outlines a method where SNR data are modeled to estimate these multipath parameters as time-varying quantities. The proposed method draws strongly from the algorithms used by *Comp* [1996] and *Comp and Axelrad* [1997].

[9] The following steps progress from SNR as reported by the GPS receiver (S) to carrier phase multipath corrections ($\delta\phi$). First, the SNR profile is separated into two parts: the SNR due to the direct signal, and the SNR due to multipath. The SNR from the direct signal provides an estimate of the direct amplitude, and the residual SNR due to multipath is employed in subsequent analysis stages. Next, the dominant multipath frequency as a function of time is determined via wavelet analysis. The sign of each multipath frequency is determined by limiting the analysis to multipath reflections off of flat ground or moderately tilted surfaces. Each time-localized estimate of multipath frequency is then used in an adaptive least squares process to estimate the multipath relative phase and multipath amplitude. Once the multipath parameters A_d, A_m, and ψ have been determined, equations (1)–(2) are applied to construct carrier phase corrections for multipath errors while also reconstructing the SNR profile as a check on the estimation process. Although based upon the earlier work of *Comp* [1996] and *Comp and Axelrad* [1997] the process described here has a few key changes and simplifications: estimation of multipath frequencies via wavelet analysis, modeling only single-antenna and single-reflector multipath, and incorporating assumptions of satellite-receiver geometry.

[10] The method described in this study is only applicable to receiver models that report SNR data in a way consistent with the simplified multipath model described above. We note that it is likely that many high-quality receivers implement some sort of proprietary multipath mitigation strategies at the tracking level which would alter or negate the simplified multipath model proposed here. However, it is difficult to confirm which GPS receiver models obey the above SNR-multipath relationships without knowledge of how the SNR quantity is computed within the receiver hardware and firmware, and receiver manufacturers are often reluctant to provide this information. This study uses SNR quantities recorded by the receiver and reported in RINEX files. When available in RINEX, SNR are reported as observable types S1 and S2 and record "raw signal strengths or SNR values as given by the receiver for L1, L2 phase observations" [*Gurtner*, 1994]. SNR data quality analysis by *Bilich et al.* [2007] indicates that the Ashtech Z-12 receivers report SNR for the L1 phase that are consistent with the simplified multipath model, therefore L1 Ashtech Z-12 data are used in this study.

3.1. Signal Component Separation

[11] For a single satellite, the SNR reported by the receiver $S(t)$ can be modeled as the sum of the SNR due to the direct signal and the SNR due to multipath, respectively denoted $\bar{S}$ and δS. The SNR time series for each satellite must be separated into these direct and multipath components for two reasons: to obtain an estimate of the direct amplitude and to remove the largest amplitude trend from the SNR data, the latter of which increases robustness of the spectral analysis and estimation stages.

[12] The overall magnitude trends of $\bar{S}$ and δS are largely determined by the receiving antenna's gain pattern (Figure 2a). For satellites observed at positive elevation angles, most geodetic antenna gain patterns will yield a direct signal SNR time series with maximum amplitude when the satellite reaches its apex (Figure 2b). In contrast, most multipath geometries will reflect the signal in such a way that the reflected signal will pierce the gain pattern at negative elevation angles, resulting in smaller signal amplitudes than $\bar{S}$ and maximum multipath amplitudes at the arc extremities (Figure 2b).

[13] Based upon the variable gain of direct and multipath signal components, this study assumes that long-period, very large amplitude oscillations in the $S(t)$ of an entire satellite pass are due to the direct signal. The direct signal SNR is modeled by fitting a polynomial of order 5–15 to each $S(t)$ series; removing this polynomial leaves $\delta S(t)$, which is used in subsequent stages.

3.2. Signal Conditioning

[14] Next, the quality of each δS time series is evaluated and poor quality data are eliminated from further analysis stages. For the Ashtech Z-12 receivers and firmware used in this study, the SNR data were reported with 0.1-dB precision. When SNR data of this precision are converted to amplitude units on a linear scale (volts), the quantization levels become compressed for small dB values but are inflated for the large dB values, with differences of several volts for some adjacent values. Removing the direct signal component of SNR results in a δS time series with significant

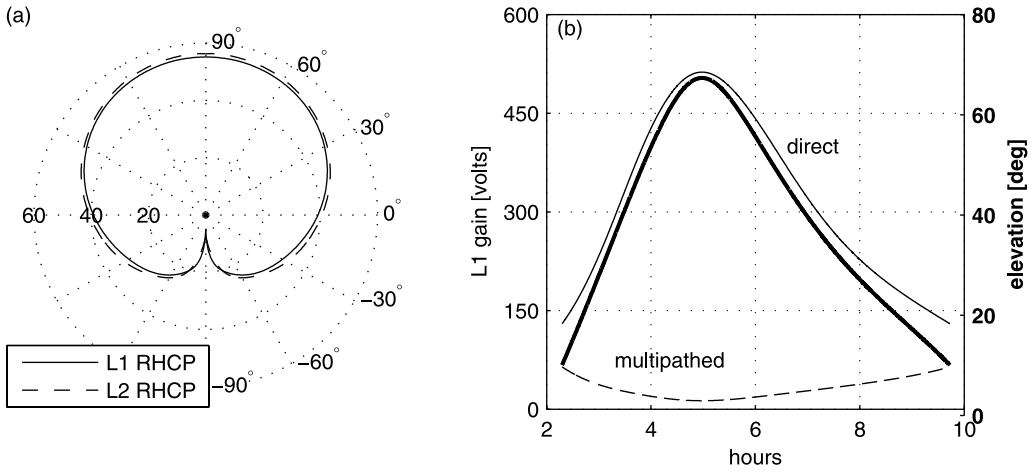

Figure 2. Relationship between receiving antenna gain pattern and the amplitude of direct and multipath signals. (a) Gain patterns for L1 and L2 right-handed circularly polarized (RHCP) signals for an Allen-Osborne Dorne/Margolin chokering antenna, in dB; the outer ring of elevation angle labels assumes the antenna is mounted parallel with local horizontal. (b) Expected direct (light solid line) and multipath (dashed line) amplitudes assuming a single reflection from an infinite horizontal surface below the antenna given the theoretic satellite elevation angle profile (heavy line). For (b), gain values from (a) are converted to volts ($V = 10^{dB/20}$).

high-elevation sections that are now distorted (Figure 3b) and have the false appearance of oscillatory multipath behavior. At high satellite elevation angles the chokering antenna gain pattern dictates that $A_m \ll A_d$, thus any multipath signature will be so small as to be obscured or misrepresented by the quantization distortion. Therefore in this analysis, data above 30° are thrown out to eliminate the distorted data sections. In conjunction with removing problematic SNR data from consideration, each satellite arc is separated into its ascending and descending components.

[15] Note that multipath effects are largest at the ends of the arc where $A_m \ll A_d$, therefore multipath effects that we need to analyze will be greatest at the same time that edge effects might lead to improper parameter estimation. To avoid edge effects, each individual ascending and descending SNR time series is padded. The method of *Kijewski and Kareem* [2002] is adopted, where both ends of a $\delta S(t)$ series are padded with a negative, reversed order version of the same series. This type of signal padding enables accurate parameter estimation at the extremities of each time series.

3.3. Frequency Estimation

[16] To determine the carrier phase multipath error, the phase of the multipath signal relative to the direct signal ψ must be estimated. In subsequent discussion, estimated quantities are denoted by the ($\wedge$) symbol over a variable. Note that the time-varying nature of ψ generates oscillations in both SNR and carrier phase error (equations (1)–(2)) as these quantities are dominated by the cosine or sine of ψ, respectively. Thus the oscillatory behavior of SNR is defined by the rate of change of ψ, i.e., $\omega \equiv d\psi/dt$. We estimate $\omega(t)$ (equation (6)) from the $\delta S(t)$ profile and use these time-varying estimates of the predominant multipath angular frequency to compute $\hat{\psi}(t)$ in a subsequent analysis stage.

[17] In this study, estimates of the SNR frequency $\hat{\omega}(t)$ are determined via wavelet transform [*Torrence and Compo*, 1998]. The wavelet transform method was chosen as it can be used to analyze time series with non-stationary power at different frequencies, as is the case for multipath. In addition, the wavelet transform yields estimates at every

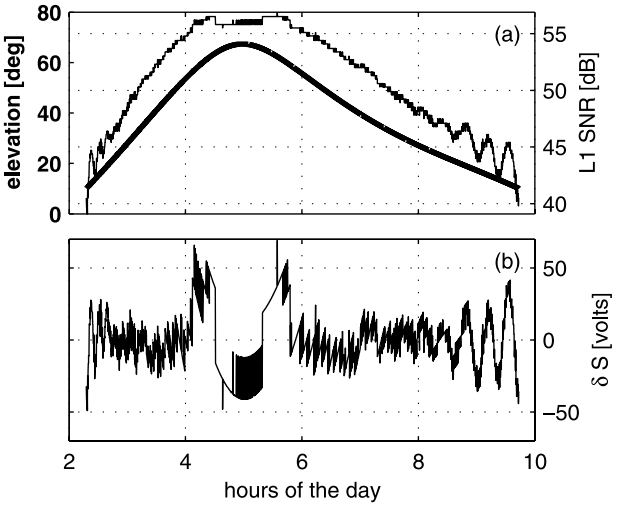

Figure 3. Demonstration of the data quality and general absence of multipath oscillations at high elevation angles, using UYT2 Ashtech Z-12 for PRN8 on 10 September 2002. (a) SNR data as reported in the RINEX file with units of dB (light line), and the corresponding elevation of the satellite (bold line and axis) as a function of time. (b) δS profile after converting the original SNR data to volts and removing a 9th order polynomial. Note that data between hours 3 and 8.5 (above 30°) have a jagged character that obscures any possible multipath signature.

epoch, which is necessary for error profile computation. To compute the continuous wavelet transform W_n, each padded δS time series of length N samples and sampling interval δt is convolved with the wavelet function Ψ:

$$W_n(s) = \sum_{n'=0}^{N-1} \delta S_{n'} \Psi^* \left[\frac{(n'-n)\delta t}{s} \right] \quad (7)$$

where the asterisk (*) is the complex conjugate operator. In the wavelet transform, a wavelet of scale s is essentially translated along the time index n to ascertain the time-varying frequency and power of features in the time series. The continuous wavelet transform is approximated using the Fourier transform as outlined by *Torrence and Compo* [1998]. This study uses the Morlet wavelet, a sinusoid modulated by a Gaussian, as the wavelet function Ψ. The Morlet wavelet has both real and imaginary parts, therefore we represent the amplitude of the wavelet transform using the wavelet power spectrum $|W_n(s)|^2$, a real-valued quantity.

[18] The choice of wavelet scales determines the resolvable frequencies. In this study, the wavelet transform is computed over scales

$$s_j = s_0 2^{j\delta j}, \quad j = 0, 1, \ldots, J \quad (8)$$

$$J = \delta j^{-1} \log_2 (N\delta t / s_0) \quad (9)$$

where $s_0 = 2\delta t$ is the smallest scale and J is the largest. A spacing between scales of $\delta j = 0.15$ was chosen as this value yielded sufficiently fine frequency resolution for slowly varying multipath. Equation (8) leads to discrete wavelet scales which are further apart as the wavelength increases, that is for the longest periods or lowest frequencies. At every epoch, the scale with maximum wavelet power is assumed to be the dominant multipath contributor, and that scale s is subsequently converted to an equivalent Fourier period or frequency. For any wavelet, the wavelet scale can be directly related to the Fourier frequency ω [*Meyers et al.*, 1993]; for the Morlet wavelet $\omega = 0.97s$.

[19] Before proceeding to amplitude and phase estimation, the sign of the frequency values must be adjusted. The SNR, the oscillatory time dependence of which is driven by $\cos(\psi)$, is insensitive to the sign of the change in multipath phase, thus wavelet analysis yields frequency values that have no connection to the sign of ω. However, the $\sin\psi$ term in the denominator of equation (1) means that incorrect determination of the sign of ω and therefore $d\psi/dt$ will yield an inverted phase correction profile, essentially doubling the potential multipath error instead of removing it. Assuming horizontal reflecting surfaces and forward scattering (equation (6)) allows us to avoid this pitfall by establishing that changes in ψ and θ with time will have equivalent sign. Thus the sign of $\hat{\omega}$ is adjusted to be consistent with that of $d\theta/dt$, i.e., the ascending ($+\hat{\omega}$) or descending ($-\hat{\omega}$) portion of a satellite arc, before estimating the multipath parameters.

3.4. Multipath Parameter Estimation

[20] Adaptive least squares, hereafter referred to as ALS, allows dynamic determination of amplitude and phase as a function of time. In this implementation, the ALS is initialized with the frequency estimates $\hat{\omega}$ from the above wavelet analysis and operates on the SNR data after the direct signal has been removed. In theory, it is possible to estimate the multipath frequency ω in addition to A_d, A_m, and ψ using only δS as an input, but the ALS method is insufficiently robust to estimate ω in the presence of noise [*Comp*, 1996]; initializing the ALS with $\hat{\omega}$ increases ALS robustness and aids convergence of the multipath parameter estimates.

[21] The ALS estimates the multipath parameters by modeling δS as a cosine C in the presence of noise ε with a time-varying mean offset of A_0 that accounts for the imperfect nature of the polynomial removal:

$$\delta S(t) = A_0(t) + C + \varepsilon$$

$$\delta S(t) = A_0(t) + A_m(t)\cos\psi(t) + \varepsilon \quad (10)$$

Equation (10) is given as a function of time t, where A_m is the multipath amplitude and ψ is the multipath relative phase. Although ALS can estimate multiple multipath contributions at once, this study solves for a single dominant reflector.

[22] The ALS operates on this linear model of periodic signals embedded in noise (equation (10)). The multipath relative phase is a function of the time-varying multipath frequency (provided by wavelet analysis, here in radians), assumed to be constant from one epoch to the next:

$$\psi(t_k) = \hat{\omega}(t_{k-1})\delta t + \psi(t_{k-1}) \quad (11)$$

The state vector at any epoch $v(t_k)$ is composed of sine (in-phase) and cosine (quadrature) components for each periodic signal, plus an additional element to estimate any mean offset A_0:

$$v(t_k) = \begin{pmatrix} 1 \\ v_s \\ v_c \end{pmatrix} = \begin{pmatrix} A_0 \\ A_m(t_k)\sin\psi(t_k) \\ A_m(t_k)\cos\psi(t_k) \end{pmatrix} \quad (12)$$

The orthogonal sine and cosine components are included in the state pair so that A_m and ψ can be separately determined. From one time to the next, the state estimate is propagated by the transition matrix,

$$\Phi(t_k, t_{k-1}) = \begin{bmatrix} 1 & 0 & 0 \\ 0 & \cos(\omega(t_{k-1})\delta t) & \sin(\omega(t_{k-1})\delta t) \\ 0 & -\sin(\omega(t_{k-1})\delta t) & \cos(\omega(t_{k-1})\delta t) \end{bmatrix} \quad (13)$$

Starting at high satellite elevation angles (low multipath) and moving toward the lower elevations (high multipath), the state is sequentially updated via least squares under the minimum variance criteria. In this adaptive implementation of least squares a forgetting factor is applied to discount old measurements when updating the state and error covariance; forgetting factors of 0.99 for A_0 and 0.95 for ψ are used in

Table 2. Station Locations and Baseline Lengths for the Salar de Uyuni Data Set[a]

Station	Latitude, deg	Longitude, deg	Height, m	Δh, m
Center	−20.211	292.577	3697.0	
UYT1	0.7854e-3	0.4398e-3	0.316	0.009
UYT2	0.8405e-3	0.3122e-3	0.336	1.442
UY04	0.8886e-3	0.4680e-3	0.320	0.009
$Station_1$	$Station_2$	Distance, m		
UYT1	UYT2	14.67		
UYT1	UY04	11.81		
UYT2	UY04	17.14		

[a]Station positions are relative to the 'center' location. Δh is the antenna height above the salt flat (ground) and is relative to the station position.

this study. A more detailed explanation of ALS is given by *Bilich* [2006] and *Comp* [1996].

[23] The desired estimates of multipath amplitude and relative phase come from the magnitude and phase of the updated orthogonal state pair:

$$\hat{A}_m(t) = \| \hat{v}(t) \| = \sqrt{\hat{v}_s^2(t) + \hat{v}_c^2(t)} \tag{14}$$

$$\hat{\psi}(t) = \arctan\left(\frac{\hat{v}_s(t)}{\hat{v}_c(t)}\right) \tag{15}$$

3.5. Multipath Profile Construction

[24] The combined wavelet and ALS method provides estimates of residual direct amplitude $\hat{A}_0(t)$, multipath amplitude $\hat{A}_m(t)$, and multipath relative phase $\hat{\psi}(t)$ all as a function of time. The residual direct amplitude is added to the direct amplitude estimate from the signal separation stage to create the final estimate of $\hat{A}_d(t)$:

$$\hat{A}_d(t) = \bar{S}(t) + \hat{A}_0(t) \tag{16}$$

These three multipath parameter estimates are all that is necessary to construct phase multipath corrections. Substituting these estimates into equation (1):

$$\delta\hat{\phi}(t) = \arctan\left(\frac{\hat{A}_m(t)\sin\hat{\psi}(t)}{\hat{A}_d(t) + \hat{A}_m(t)\cos\hat{\psi}(t)}\right) \tag{17}$$

This estimate of the phase error due to multipath $\delta\hat{\phi}(t)$, in radians, can be used to correct GPS phase data corrupted by multipath errors. Multiplication by $\lambda/2\pi$ converts the phase error into distance units so that the magnitude of the phase error can be understood in terms of a range error.

[25] An estimated SNR profile $\hat{S}(t)$ serves as a check on the multipath parameter estimates; if significant differences exist between the raw SNR data and the reconstructed or estimated SNR profile, the estimates of one or more multipath parameters is in error. From equation (2), the composite SNR, which includes both direct and multipath effects, is:

$$\hat{S}(t) = \sqrt{\hat{A}_d^2(t) + \hat{A}_m^2(t) + \hat{A}_d(t)\hat{A}_m(t)\cos\hat{\psi}(t)} \tag{18}$$

Because the SNR due only to multipath contains the most variation and has no dependency on direct multipath amplitude, constructing an estimate of the SNR due to multipath can be a useful check on $\hat{\psi}$ and $\hat{A}_m$:

$$\delta\hat{S}(t) = \hat{A}_m(t)\cos\hat{\psi}(t) \tag{19}$$

4. Salar de Uyuni Experiment

[26] A valuable GPS multipath data set was collected on the Salar de Uyuni, a large salt flat on the Bolivian Altiplano. The original purpose of this experiment was to provide ground truth data for the IceSat mission [*Borsa*, 2005; *Borsa et al.*, 2007], but the sub-decimeter topography and relatively uniform ground composition create a large horizontal reflecting surface well-suited to multipath study. This experiment involved a 3-station network of Ashtech Z-12 GPS receivers operating with Ashtech Dorne/Margolin model chokering antennas, with 11-17 m baselines between the three GPS stations (Table 2). Two antennas (UYT1 and UY04) were mounted flush with the ground; station UYT2 was located on a tripod mount approximately 1.4 m above the surface. Figure 4 illustrates the experimental setup.

[27] The three-station network allows easy assessment of the characteristics of multipath-free versus multipath-corrupted position solutions. The characteristics of multipath-free results are established by solutions for UYT1 relative to UY04. Because both of these antennas are flush with the ground, they should not experience significant ground multipath. In contrast, a two-station solution with UYT2 (tripod-mounted) and UY04 (ground-mounted) should be heavily corrupted by multipath errors. Postfit phase residuals for each station pair are single-differenced to account for the least squares distribution of error in each solution.

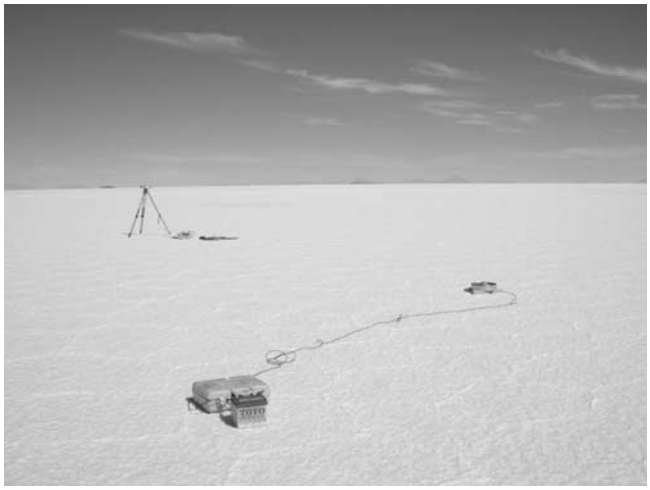

Figure 4. The Salar de Uyuni of Boliva, a 9000 km^2 salt flat in South America. This photo displays the experimental setup of UYT2 (tripod-mounted antenna) and UY04 (antenna flush with the ground); the setup of UY04 is analogous with UYT1 (not shown), located at a similar distance from UYT2 (Table 2).

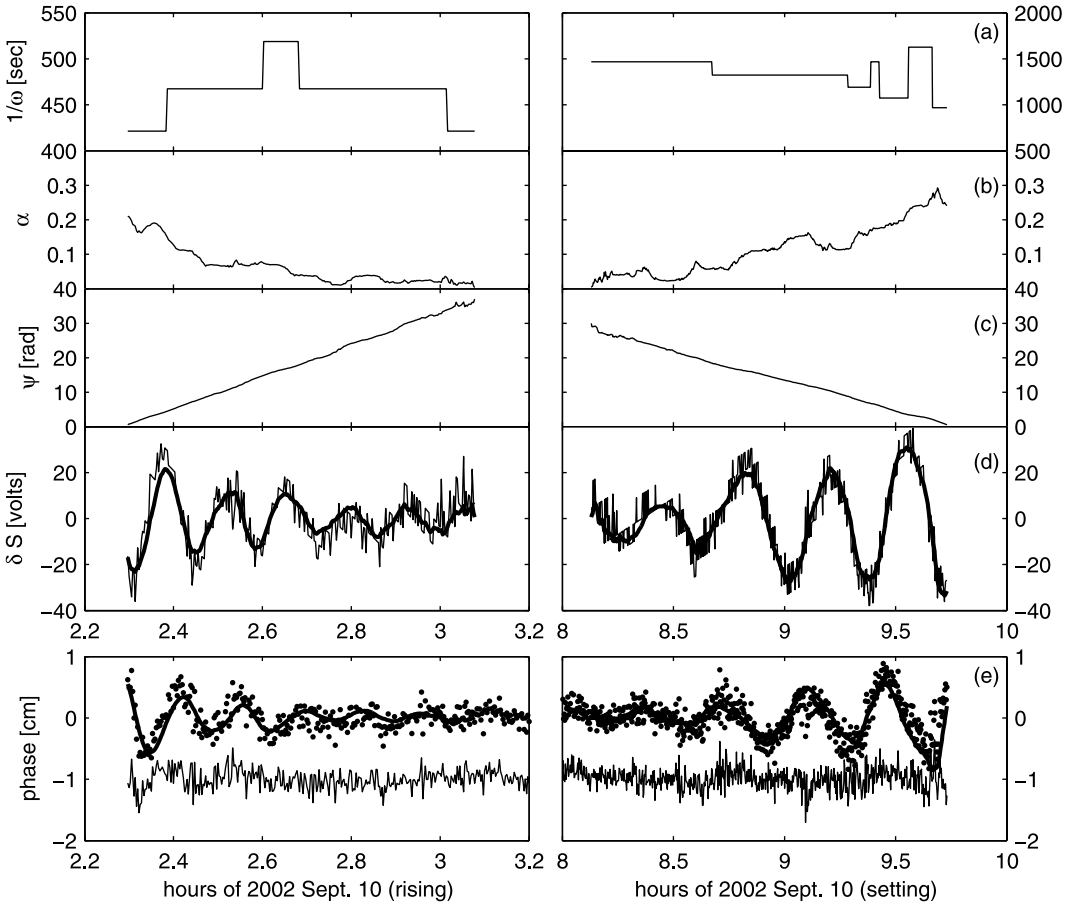

Figure 5. Results of the combined wavelet-ALS algorithm for PRN8, station UYT2, 10 September 2002, where the results shown are all between 10 and 30° elevation. The lefthand column contains the ascending or rising pass results, whereas the righthand column contains the descending or setting pass, all as a function of time. (a) $\hat{\omega}$ from wavelet analysis, expressed as a period (in seconds); (b) $\alpha = \hat{A}_m/\hat{A}_d$ from ALS; (c) unwrapped $\hat{\psi}$ from ALS; (d) δS input data (light line) with reconstructed SNR profile (heavy line) using the $\hat{A}_d$, $\hat{A}_m$ and $\hat{\psi}$ estimates from above; (e) phase corrections and their effect on double-differenced L1 phase: dots = original double-differenced phase $dd\phi$, heavy line = phase correction $\delta\phi$ from multipath parameter estimates, light line = double-differenced phase after corrections have been applied. Double-differences were formed using PRN13 for ascending and PRN23 for descending PRN8 segments.

[28] Ten hours of data collected at 10 s sample intervals on 10 September 2002 were used in this study. The GPS data were collected with a 10° elevation mask, and all recorded data are included in the analysis. Data were analyzed two stations at a time in network mode with the GIPSY software [*Lichten and Border*, 1987] and precise IGS orbits [*Dow et al.*, 2005] in the International Terrestrial Reference Frame (ITRF) 2000 [*Altamimi et al.*, 2002]. In all solutions discussed here, the position of UY04 is tightly constrained (σ = 1.0 cm), a second station serves as the reference clock, and 100% of phase biases were resolved [*Blewitt*, 1989]. In early analysis it was noted that some of the multipath error for the tripod station would be redistributed to the wet troposphere estimate instead of the residuals or positions. To prevent this behavior, the wet troposphere delay was estimated as a random walk process ($\sigma = 5.0 \times 10^{-8}$ km/$\sqrt{s}$) using the ground-only network, then input to the tripod (multipath) solutions before and after corrections were implemented. The short baselines involved permit computation of single-frequency L1 solutions instead of requiring the traditional dual-frequency (L1 and L2) ionosphere-free solution. Because of questionable L2 SNR data quality [*Bilich et al.*, 2007], only the L1 SNR data were used to generate corrections.

4.1. Phase Multipath Estimation

[29] Corrections were developed using the combined wavelet-ALS algorithm, which was applied to all satellites tracked at station UYT2 on 10 September 2002. Only data between 10 and 30° elevation were used, resulting in 20 satellites and a total of 30 ascending and descending arc segments available for analysis. Under these restrictions, multipath phase corrections were applied to approximately 40% of the data points in the 10-h solution.

[30] Figures 5 and 6 present representative examples of estimated parameters and the resultant phase corrections. In

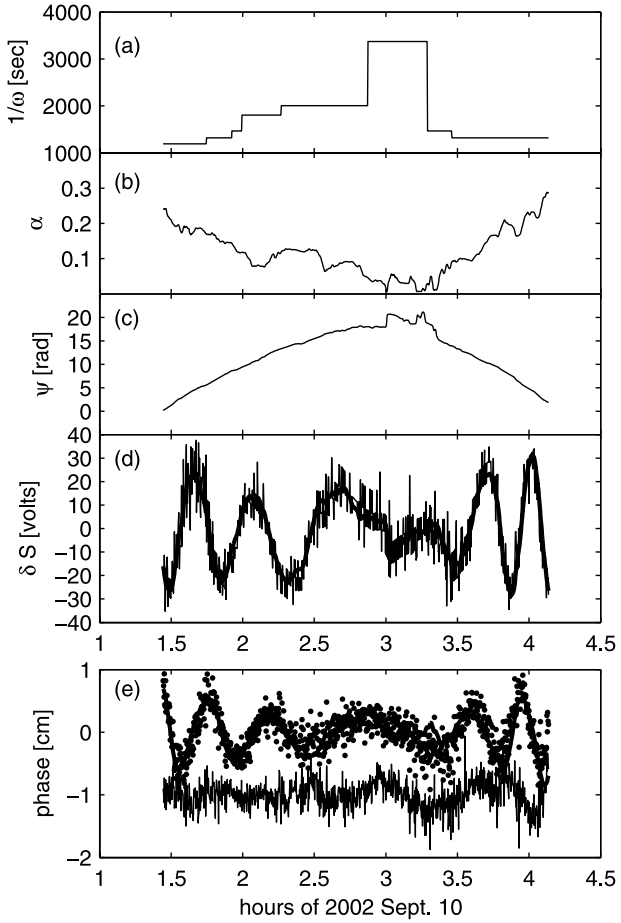

Figure 6. Results of the combined wavelet-ALS algorithm for PRN2, station UYT2, 10 September 2002, a satellite pass which remained below the 30° elevation cutoff. The double-difference $dd\phi$ was formed using PRN13. See also Figure 5.

each figure, the $\hat{\omega}$ from wavelet analysis is provided to demonstrate the distribution of frequencies typical for this data set. The estimates of multipath parameters $\hat{A}_0$, $\hat{A}_m$ and $\hat{\psi}$ come from the ALS estimation stage, and equation 16 yields the final $\hat{A}_d$ value. Phase corrections (equation (17)) and SNR due to multipath (equation (19)) are computed from these parameter estimates, with the latter serving as a check on the estimation process. In addition, double-differenced phase observables $dd\phi$ for the UYT2-UY04 baseline are included to directly assess the phase errors due to multipath. Because of the short baselines between receivers, several simplifying assumptions (equivalent tropospheric delay; ionospheric delay approximated as a low-order polynomial; satellite geometric range differences equivalent to station baseline length) were used [*Hoffmann-Wellenhof et al.*, 1997]. To isolate the multipath error of a single satellite observed at UYT2, the satellite pairs used to form $dd\phi$ are selected so that the satellite of interest is at low elevation (large multipath) and the other satellite is at a high elevation (relatively multipath-free). After applying the $\delta\hat{\phi}$ corrections to the UYT2 phase data, the double differences are recomputed; with proper correction profiles, the majority of structured noise should have been removed from the new $dd\phi$ profile.

[31] Results from PRN8 (Figure 5) are typical of most satellites in this data set. Frequency estimates from wavelet analysis show some variability due to different satellite elevation angle rates of change for the ascending and descending passes, and quantization due to the discrete nature of wavelet scales (equation (8)). After passing these wavelet analysis frequencies to the ALS the resulting relative phase (ψ) values are quite smooth, indicating that variable frequency estimates did not adversely affect the ALS estimation. Multipath amplitude estimates vary with time, with α increasing toward the ends of the arc, yet some oscillatory structure is superimposed on this trend due to the interplay between phase and amplitude estimates. Overall, the $\delta\hat{S}$ and $\delta\hat{\phi}$ profiles correspond very well to the δS and $dd\phi$, respectively. After phase corrections were applied to UYT2, most of the structured noise has been removed from the differenced phase and the double-differenced phase RMS has been reduced by 35%.

[32] Two satellites (PRN 2 and 7) had passes which did not reach 30° elevation; the ascending and descending segments of these arcs were analyzed with a single pass of the wavelet-ALS algorithm to maintain continuity of corrections for the entire arc. As demonstrated by PRN2 (Figure 6), the multipath periods lengthen as the satellite reaches its apex at 3.0 h. As the satellite begins to descend, the sign of $d\omega/dt$ changes, which leads to temporary ψ tracking issues that end as soon as the ALS begins processing larger amplitude, shorter period oscillations. Despite these issues, multipath and direct amplitude estimates still

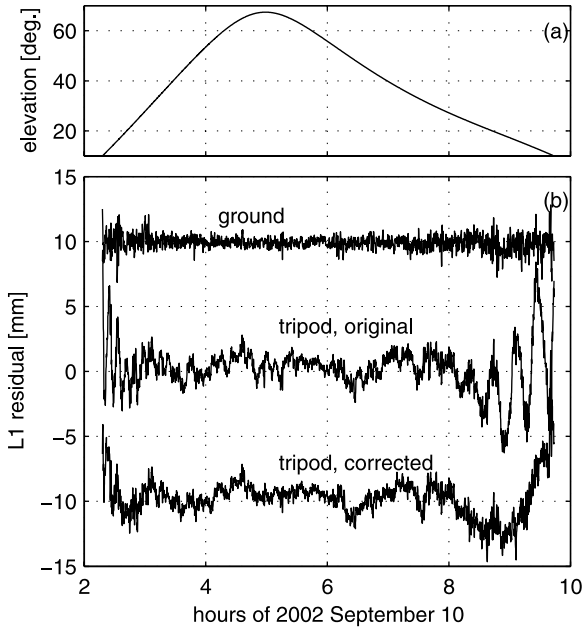

Figure 7. Example of 10 s L1 phase residuals as a function of time for PRN8/GPS38 on 10 September 2002; residuals were smoothed with a symmetric 30 s boxcar. (a) Satellite elevation angle relative to UY04. (b) Single-differenced residuals for PRN8 for the multipath-free (ground) and multipath-corrupted (tripod) solutions. Tripod (UYT2) residuals are shown before and after implementing phase multipath corrections.

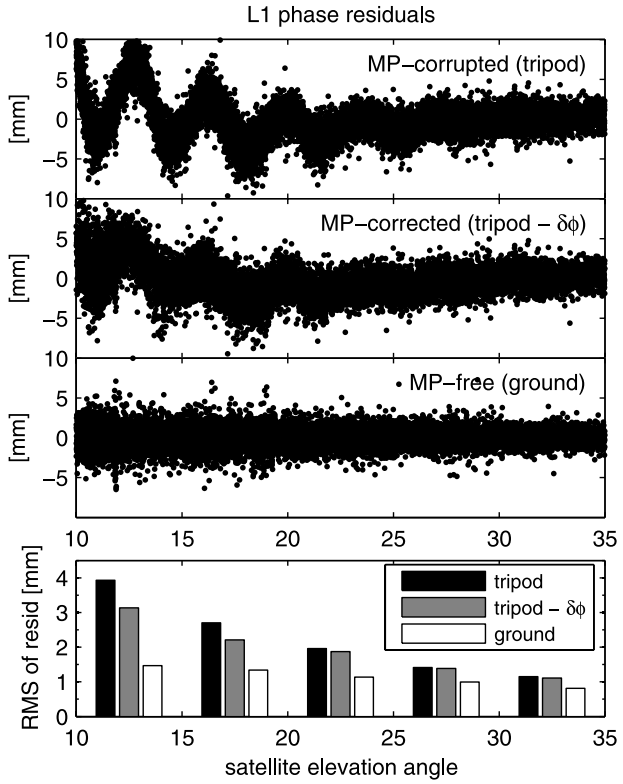

Figure 8. Trends in L1 single-differenced phase residuals as a function of satellite elevation angle for multipath-free, multipath-corrupted, and multipath-corrected solutions. All satellites in view during the analysis period are included and superimposed. Tripod residuals refer to the UYT2-UY04 baseline, whereas ground residuals come from the UYT1-UY04 solution. The bottom panel shows a histogram of the RMS of all residuals contained within a 5° bin for the three solutions.

increase and decrease, respectively, toward the ends of the arc and result in large α at the lowest elevation angles. Although the reconstructed SNR profile matches the input δS, the phase correction profile appears somewhat out-of-phase for the descending part of the arc. Even with these difficulties, the RMS of the double-differenced phase is reduced 31% by implementing the phase corrections as shown.

4.2. Positioning Results

[33] To assess the impact of multipath phase corrections, UYT2 solutions are contrasted before and after implementing corrections. Solutions computed with ground-mounted antennas, assumed to be multipath-free, are used as a target for ideal correction of carrier phase multipath at the tripod-mounted station. Two different solution types are analyzed: static positioning, where all data for the 10-h time period yield a single position estimate and all residual error will appear in the postfit residuals, and kinematic positioning at the data sample rate of 10 s, where phase error will propagate into the position estimates.

[34] When estimating a single position from all available data, errors such as multipath are largely distributed to the residuals; residuals from multipath-free and multipath-corrupted solutions are compared to understand the magnitude, frequency, and elevation angle dependence of phase multipath error as it propagates into the position solution. An example from PRN8 illustrates the primary differences between each solution's residuals (Figure 7). Large-amplitude oscillations are observed in the UYT2 (tripod) residuals while the UYT1 (ground) residuals appear to be largely white noise with slight elevation angle dependence of noise magnitude. Taking all residuals from the 10-h time period together (Figure 8) establishes the dominant trends. The ground-mounted antennas have a relatively uniform root-mean squared (RMS) error of 1.0–1.5 mm at all elevation angles. In contrast, the tripod-mounted antenna experiences significant ground-bounce multipath error; the largest amplitude errors occur at low elevation angles, with the majority of the error below 30° elevation and a 40–170% increase in RMS relative to the ground residuals.

[35] Implementing L1 multipath corrections for UYT2 phase data leads to substantial improvement of the residuals. The sinusoidal signatures are largely eliminated (Figures 7 and 8) with a ~19% reduction in RMS for data below 20° elevation and all satellites. The phase corrections successfully reduce systematic errors in the residuals over 200–2000 s periods (Figure 9). However, some errors are still present in the residuals after implementing the corrections, notably a non-zero trend over 10–20° which is not explained by the single-reflector SNR multipath model.

[36] Because the antennas were stationary during the 10-h site occupation, any non-zero measurements observed in positions estimated kinematically (at every epoch) are the result of unmodeled errors such as multipath. For the ground-mounted antennas, kinematic positions maintain zero mean over the 10-h period with white noise characteristics over 20–2000 s periods in all components (Figure 10), thereby establishing a benchmark for multipath-free positions. Positions for the antenna located 1.4 m above the ground show large amplitude systematic errors in all components, with significant non-white power at >300 s periods, consistent with ground multipath for the given antenna height. Incorporating phase multipath corrections leads to encouraging levels of error reduction. In general,

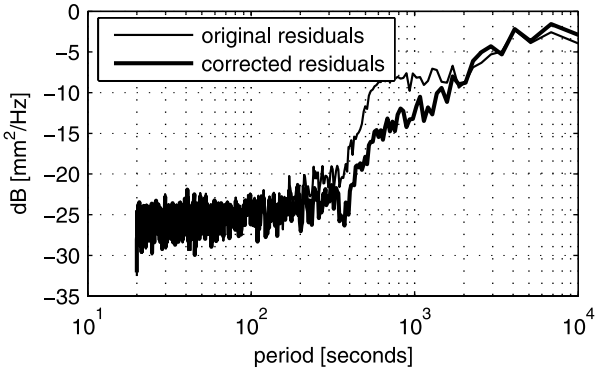

Figure 9. Mean power spectral density of the single-differenced L1 phase residuals before and after implementing L1 phase corrections to UYT2 data. Only residuals below 35° elevation are used (see Figure 8), and spectra from individual satellites are averaged.

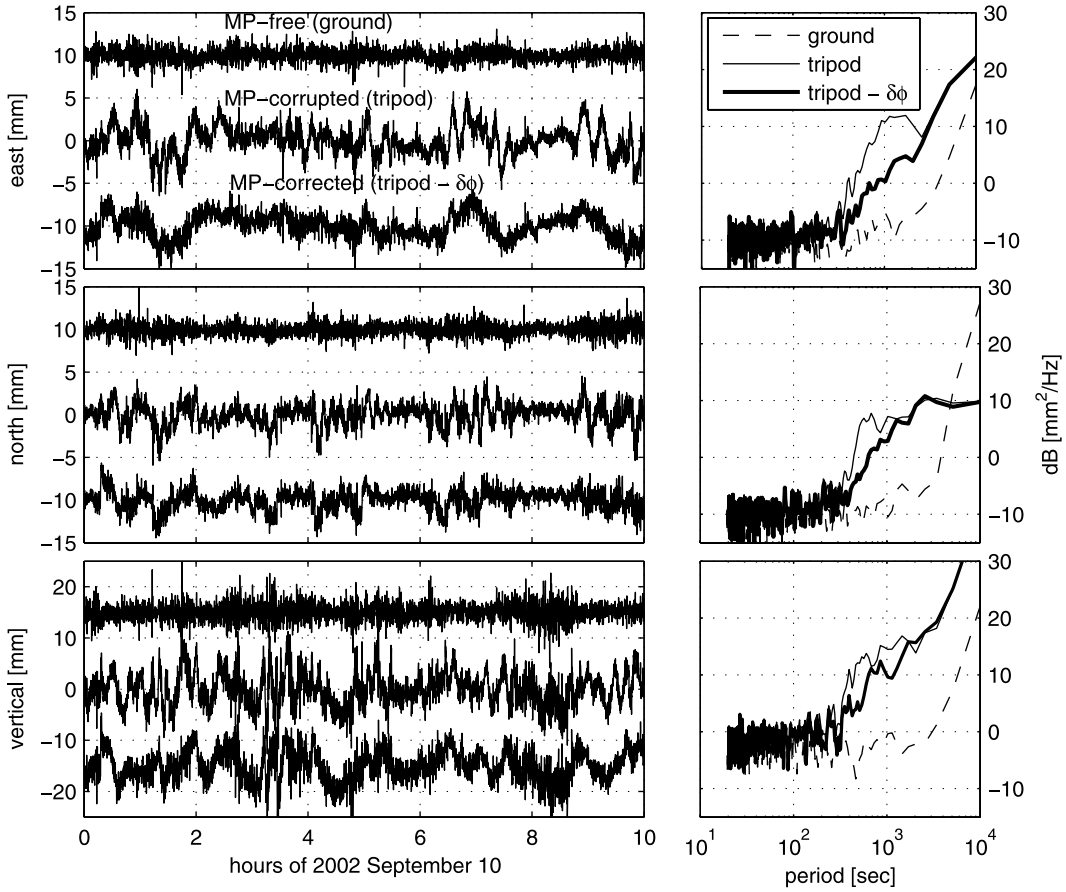

Figure 10. Stochastic positions estimated at every epoch (10 s) for all three components. Left: positions estimated for the UYT1 ground network (top trace) are contrasted with the UYT2 positions before (center) and after (bottom) implementing phase multipath corrections. Right: Power spectral density estimates via Welch's method (average of periodograms for eight data sections with 50% overlap) in dB of mm^2/Hz for each of the traces on the left. Note the reduction in power at 300–2000 s periods for all components.

the multipath corrections decrease but do not completely remove systematic errors in the position series. Most power reduction occurs at the expected multipath amplitudes of 300–2000 s, with the greatest amount of power reduction in the east component, followed by the north then vertical components, on the order of 1 to 7 dB. Despite these increases in whitening the error spectrum of multipath-prone phase measurements, systematic errors still remain with much greater power than the ground-mounted antennas.

5. Conclusions

[37] This paper models GPS carrier phase multipath error using signal-to-noise ratio (SNR) data. Theory states that the time-evolving nature of multipath will lead to oscillations in both measured carrier phase and SNR data which have the same frequency but are out-of-phase. By estimating the dominant frequencies and amplitudes represented in SNR data, quantitative measures of multipath error in phase data can be derived.

[38] We present a method for determining absolute multipath at a single station that is based upon previous theory for differential multipath from closely spaced multiantenna arrays. For the single station application, additional simplifying assumptions specific to characteristics of geodetic GPS installations were made, from common satellite-receiver geometries to the likely geometry of reflecting surfaces. The SNR-multipath modeling method of this study used the wavelet transform to estimate the non-stationary spectral content of a SNR time series, then passed the frequency estimates to a filter that implemented adaptive least squares (ALS) to estimate multipath parameters such as the amplitude and relative phase. Multipath corrections for carrier phase data were derived from these parameter estimates and were then applied to the raw, multipath-corrupted phase measurements. One notable advantage of the technique described here is that contemporaneous data streams were used to generate the multipath corrections; unlike methods such as sidereal filtering or aspect repeat time adjustment [e.g., *Larson et al.*, 2007; *Choi et al.*, 2004] which require multiple consecutive days of data, this method is well-suited to mitigating multipath effects in campaign data where limited time is spent occupying the GPS site.

[39] This technique was applied to data collected on the Salar de Uyuni, a salt flat in Bolivia which serves as an

horizontal reflecting surface of large extent and negligible topography with uniform reflecting characteristics. Contrasting solutions before and after applying multipath corrections shows that phase errors are removed at periods consistent with ground multipath reflections, with a 20% reduction in postfit residuals RMS at low elevation angles (data <20° elevation) and reduced spectral power in kinematic positions. This level of improvement is consistent with earlier SNR modeling work using differential arrays [e.g., *Comp and Axelrad*, 1997; *Ray and Cannon*, 2001]. Although the amount of improvement is considerable, contrasting these multipath-corrected with multipath-free solutions shows that the magnitude of corrections is insufficient to consider the corrected observables 'multipath-free'.

[40] Although the ideal relationship between SNR and phase multipath is well defined in theory, several factors limit the applicability of the SNR phase multipath modeling technique in practice. Of primary importance, it is expected that most high quality receivers implement proprietary multipath mitigation strategies at the tracking or observable computation phase. Multipath mitigation at the hardware or firmware level would alter or negate the simplified SNR-multipath model proposed here. Similarly, we note that other factors affect SNR and carrier phase but do not obey the same relationships as multipath; if, for example, SNR oscillations due to antenna phase center variations or antenna gain pattern ripples were modeled as multipath-induced phenomena, implementing phase corrections would only further corrupt position solutions. Likewise, the direct and multipath components of SNR must be properly separated to avoid mistaking residual direct signal as multipath. Finally, a generalized version of this technique would have to account for multiple reflecting objects of finite extent and different orientations. To use the technique presented in this study, these general environments would be separately modeled by iterations of the wavelet-ALS algorithm. Initial research into more complicated multipath environments indicates that contributions from multiple reflecting objects must have markedly different frequencies for wavelet-ALS iteration to be effective, a condition which is seldom met in actual antenna environments.

[41] Additionally, SNR data quality will impact the efficacy of the modeling process. The SNR data themselves must be estimated from the tracking loop outputs in such a way that oscillations in SNR are of equivalent frequency to oscillations in the phase error. Each SNR value must also be reported with sufficient precision for spectral analysis to properly resolve the constituent frequencies. However, experience with many stations, receiver models, and phase data on different GPS frequencies shows this is not always the case [*Bilich et al.*, 2007].

[42] Our experience in applying this technique to additional stations and receiver types indicates that extracting multipath amplitude and phase information from SNR time series is a difficult process requiring heavy levels of user input, data editing, and careful station selection. Nevertheless, the encouraging results from the Salar de Uyuni data set suggest that if SNR of high precision and accuracy were available on both frequencies for geodetic GPS sites, this method could potentially be useful for modeling and removing phase errors for simple multipath environments.

[43] **Acknowledgments.** The authors would like to thank Adrian Borsa for collecting and graciously providing the playa data set, and Duncan Agnew, John Langbein, and Christopher Comp for sharing their valuable spectral analysis knowledge. Wavelet software was provided by C. Torrence and G. Compo, and is available at URL http://paos.colorado.edu/research/wavelets/. This research was sponsored by a NSF grant on multipath (EAR-000343) and a NSF graduate student research fellowship (AB). Reviews by Jim Davis and Clement Ogaja helped improve the manuscript.

References

Altamimi, Z., P. Sillard, and C. Boucher (2002), ITRF2000: A new release of the international terrestrial reference frame for Earth science applications, *J. Geophys. Res.*, *107*(B10), 2214, doi:10.1029/2001JB000561.

Axelrad, P., K. M. Larson, and B. Jones (2005), Use of the correct satellite repeat period to characterize and reduce site-specific multipath errors, paper presented at ION GNSS 2005, Institute of Navigation, Long Beach, CA.

Bilich, A. L. (2006), Improving the precision and accuracy of geodetic GPS: Applications to multipath and seismology, Ph.D. dissertation, University of Colorado, Boulder.

Bilich, A., and K. M. Larson (2007), Mapping the GPS multipath environment using the signal-to-noise ratio (SNR), *Radio Sci.*, *42*, RS6003, doi:10.1029/2007RS003652.

Bilich, A., P. Axelrad, and K. M. Larson (2007), Scientific utility of the signal-to-noise ratio (SNR) reported by geodetic GPS receivers, paper presented at ION GNSS 2007, Institute of Navigation, Ft. Worth, TX.

Blewitt, G. (1989), Carrier phase ambiguity resolution for the Global Positioning System applied to geodetic baselines up to 2000 km, *J. Geophys. Res.*, *94*, 10,187–10,203.

Bock, Y., R. Nikolaidis, and P. de Jonge (2000), Instantaneous geodetic positioning at medium distances with the Global Positioning System, *J. Geophys. Res.*, *105*, 28,223–28,253, doi:10.1029/2000JB900268.

Borsa, A. A. (2005), Geomorphology of the salar de Uyuni, Boliva, Ph.D. dissertation, University of California, San Diego.

Borsa, A. A., J. B. Minster, B. G. Bills, and H. Fricker (2007), Modeling long-period noise in kinematic GPS applications, *J. Geod.*, *81*, 157–170, doi:10.1007/s00190-006-0097-x.

Braasch, M. S. (1996), Multipath effects, in *Global Positioning System: Theory and Applications*, edited by B. W. Parkinson, J. J. Spilker Jr., P. Axelrad, and P. Enge, vol. 1, chap. 14, American Institute of Aeronautics and Astronautics.

Choi, K., A. Bilich, K. M. Larson, and P. Axelrad (2004), Modified sidereal filtering: Implications for high-rate GPS positioning, *Geophys. Res. Lett.*, *31*, L22608, doi:10.1029/2004GL021621.

Comp, C. (1996), GPS carrier phase multipath characterization and a mitigation technique using the signal-to-noise ratio, Ph.D. dissertation, University of Colorado, Boulder.

Comp, C., and P. Axelrad (1997), Adaptive SNR-based carrier phase multipath mitigation technique, *IEEE Trans. Aerosp. Electron. Syst.*, *34*(1), 264–276, doi:10.1109/7.640284.

Dow, J. M., R. E. Neilan, and G. Gendt (2005), The International GPS Service (IGS): Celebrating the 10th anniversary and looking to the next decade, *Adv. Space. Res.*, *36*(3), 320–326, doi:10.1016/j.asr.2005.05.125.

Elosegui, P., J. Davis, R. Jaldehag, J. Johansson, A. Niell, and I. Shapiro (1995), Geodesy using the Global Positioning System: The effects of signal scattering on estimates of site position, *J. Geophys. Res.*, *100*, 9921–9934, doi:10.1029/95JB00868.

Georgiadou, Y., and A. Kleusberg (1988), On carrier signal multipath effects in relative GPS positioning, *Manuscr. Geod.*, *13*, 172–179.

Gurtner, W. (1994), RINEX: The Receiver Independent Exchange format, *GPS World*, *5*(7).

Hoffmann-Wellenhof, B., H. Lichtenegger, and J. Collins (1997), *GPS: Theory and Practice*, Springer-Verlag.

Kedar, S., G. Hajj, B. Wilson, and M. Heflin (2003), The effect of second order GPS ionospheric correction on receiver positions, *Geophys. Res. Lett.*, *30*(16), 1829, doi:10.1029/2003GL017639.

Kijewski, T., and A. Kareem (2002), On the presence of end effects and their melioration in wavelet-based analysis, *J. Sound Vib.*, *256*, 980–988, doi:10.1006/jsvi.2001.4227.

Larson, K. M., A. Bilich, and P. Axelrad (2007), Improving the precision of high-rate GPS, *J. Geophys. Res.*, *112*, B05422, doi:10.1029/2006JB004367.

Lichten, S., and J. Border (1987), Strategies for high-precision Global Positioning System orbit determination, *J. Geophys. Res.*, *92*, 12751–12762.

Mader, G. (1999), GPS antenna calibration at the National Geodetic Survey, *GPS Solut.*, *3*, 50–58, doi:10.1007/PL00012780.

Meyers, S. D., B. Kelly, and J. O'Brien (1993), An introduction to wavelet analysis in oceanography and meteorology: With application to the dispersion of Yanai waves, *Mon. Weather Rev.*, *121*, 2858–2866, doi:10.1175/1520-0493.

Ray, J. K. (2000), Mitigation of GPS code and carrier phase multipath effects using a multi-antenna system, Ph.D. dissertation, University of Calgary.

Ray, J. K., and M. E. Cannon (2001), Synergy between Global Positioning System code, carrier, and signal-to-noise ratio multipath errors, *J.Guid. Control Dyn.*, *24*, 54–63.

Reichert, A. (1999), Correction algorithms for GPS carrier phase multipath utilizing the signal-to-noise ratio and spatial correlation, Ph.D. dissertation, University of Colorado, Boulder.

Reichert, A., and P. Axelrad (1999), GPS carrier phase multipath reduction using SNR measurements to characterize an effective reflector, paper presented at ION GPS 1999, Institute of Navigation.

Springer, T., G. Beutler, and M. Rothacher (1998), A new solar radiation pressure model for the GPS satellites, *GPS Solut.*, *2*, 50–62, doi:10.1007/PL00012757.

Torrence, C., and G. Compo (1998), A practical guide to wavelet analysis, *Bull. Am. Meteorol. Soc.*, *79*, doi:10.1175/1520-0477.

P. Axelrad and K. M. Larson, Department of Aerospace Engineering Sciences, University of Colorado, Boulder, CO 80309-0429, USA.

A. Bilich, National Geodetic Survey, NOAA, 325 Broadway, E/GC2, Boulder, CO 80305, USA. (andria.bilich@noaa.gov)